Available online at www.sciencedirect.com

ScienceDirect

Journal of the European Ceramic Society 35 (2015) 179–186

www.elsevier.com/locate/jeurceramsoc

Graphene and carbon nanotube (GNT)-reinforced alumina nanocomposites

Bahareh Yazdani [a], Yongde Xia [a], Iftikhar Ahmad [b], Yanqiu Zhu [a,*]

[a] College of Engineering, Mathematics and Physical Sciences, University of Exeter, Exeter EX4 4QF, UK

[b] Center of Excellence for Research in Engineering Materials, Advanced Manufacturing Institute, King Saud University, P.O. Box 800, Riyadh 11421, Saudi Arabia

Received 16 May 2014; received in revised form 26 August 2014; accepted 29 August 2014
Available online 12 September 2014

Abstract

Alumina nanocomposites reinforced with hybrid GNTs (graphene nanoplatelets, GNPs, and carbon nanotubes, CNTs) were fabricated by hot-pressing. The effects of varied GNT contents on the microstructural features and mechanical properties of the nanocomposites were investigated. The well-dispersed GNT fillers resulted in higher sintered densities (>99%) in the composites, whilst the fracture mode alteration, grain refinement and improved strength and flexibility of the composites are associated with the CNTs and GNPs. The average fracture toughness of the nanocomposites reached up to 5.7 MPa $m^{1/2}$, against 3.5 MPa $m^{1/2}$ of the plain alumina, and the flexural strength improved from 360 MPa to 424 MPa, at a hybrid addition of 0.5 wt% GNPs and 1 wt% CNTs. Toughening mechanisms attributed with the unique morphologies and structures of the GNT fillers were also discussed based on analyses on the morphology, grain sizes and fracture mode.

Keywords: Graphene nanoplatelets; Carbon nanotubes; Al_2O_3; Nanocomposites; Toughness

1. Introduction

Among structural ceramics, Al_2O_3 is one of the most used materials in industry due to its superior hardness, chemical inertness and electrical/thermal insulation properties. These useful characteristics make Al_2O_3 suitable for a wide range of functional applications, such as high speed cutting tools,[1] dental implants, chemical and electrical insulators,[2] and armouries.[3] However, the crucially structural applications are limited by its low fracture toughness. The most promising approaches to overcoming this deficient are by way of second phase additions, such as by introducing particulates (ceramic or metal),[4–6] and long or short fibres[7,8] into the Al_2O_3 matrix. Incorporating nanoscale fillers with high tensile strength and stiffness, good flexibility, and low density into a ceramic matrix has become an interesting field of study during last decades. For example, reinforced with 1-dimensional carbon nanotubes (CNTs), some interesting improvements on the fracture toughness have been obtained for different ceramic nanocomposites.[9–15] Recently, there is a growing interest to explore the graphene nanoplatelets (GNPs) as a filler in composites, to harness their two dimensional structure with high surface area, alongside with their exceptional mechanical and electrical properties. It is expected that the two dimensional structures in GNPs will uniquely provide much higher interfacial interactions between the filler and matrix, which cannot be achieved by using any 0-dimensional nanoparticles or 1-dimensional CNTs as the filler. Recent reports have also showed such mechanical and electrical improvements in ceramic matrix nanocomposites filled with GNPs.[16–24] Thus, a hybrid filler by combining the advantages of 1-D and 2-D reinforcements may lead to further improved properties in ceramic-based nanocomposites. Indeed, this concept has recently been pioneered in polymer-based composites, which has resulted in the toughest and strongest man-made polymer composite ropes.[25–29] Inspired by this idea, to explore the effects of the hybrid reinforcement of GNPs and CNTs, namely GNTs, in a ceramic matrix is a very interesting project.

However, harder than being used in a polymer matrix, the homogenous dispersion of both CNTs and GNPs in a ceramic matrix will be the primary challenge, owing to different surface chemistry and insoluble characteristics of ceramics. As in all nanocomposites, without uniform dispersion, GNPs and CNTs

* Corresponding author. Tel.: +44 1392723620.
E-mail address: Y.Zhu@exeter.ac.uk (Y. Zhu).

http://dx.doi.org/10.1016/j.jeurceramsoc.2014.08.043
0955-2219/

will lost their unique 2-D and 1-D merits in composites. Various organic solvents, such as alcohols,[11,12,22] benzene,[28] and DMF[22] have previously been used for de-bundling CNTs and for homogeneously dispersing them in ceramic matrices. The use of such solvents may not be industrially up-scalable and environmental friendly. Most recent studies have showed that there is a steric effect between GNPs and CNTs in aqueous suspensions, which prevented the CNT agglomeration and developed highly dispersed GNP/CNT hybrid agents.[25,30]

In this study, we report the use of surfactant-assisted water to de-bundle the GNPs and CNTs that act as a hybrid filler in the Al_2O_3 matrix, in an effort to achieve improved mechanical properties in the composite.

2. Experimental

2.1. Starting materials

The CNTs used in this study, provided by Tsinghua University, China, were produced by a standard chemical vapour deposition, having an average outer diameter of 40 nm. GNPs (6–8 nm thick × 5 μm wide) were purchased from ABCR GmbH & Co, Germany. The original bohemite nanopowder (P_2), sourced from Sasol, Germany, was subject to annealing at 1000 °C for 5 h, to obtain the Al_2O_3 nanoparticles which were then used as the matrix materials. The sodium dodecyl sulphate (SDS) surfactant was purchased from Sigma–Aldrich, UK.

2.2. Powder mixing

The GNP suspension (1 mg/ml) in distilled water was first prepared with a small amount of SDS (1–2 wt% of the GNP) and dispersed with the help of an ultrasonic probe for 30 min (Sonic Processor D-100-20, Sonic system, UK). The CNTs were then chemically processed with a H_2SO_4–HNO_3 solution, to remove the residue metal catalyst. They were later dispersed into an aqueous solution containing a small quantity (<2 wt% of CNTs) of SDS, again sonicated for 30 min. The CNT slurry was incubated for 2 weeks to allow for the surfactant thoroughly adsorbed onto the CNT surfaces. 25 g of Al_2O_3 nanopowder was probe sonicated for 30 min in distilled water. In the meantime, the GNP and CNT suspensions were mixed with the Al_2O_3 suspension, which was then subject to a prolonged sonication for another 30 min. After 5 min stirring of the mixed suspension, all GNPs and CNTs were well mixed with the Al_2O_3 nanoparticles. After collection from the bottom of the beaker and dried, the powders were ready for hot-pressing. Samples are designated as $S_{x–y}$, where x refers to the GNP% content and y represents the CNT% content.

2.3. Hot-press sintering

Bulk composite samples were sintered using a hot-press furnace (S8538 UEO, FCT system, Germany) in the University of Exeter. 25 g of the pre-mixed powders was poured into the cavity of the graphite die. An external pressure of 40 MPa was applied to both ends of the die using graphite plungers, and the temperature was increased to 1650 °C at a heating rate of 10 °C/min and held for 60 min under Ar atmosphere. Samples of 50 (length) × 50 (breadth) × 2.4 (height) mm were obtained after sintering. Monolithic Al_2O_3 sample was also prepared under identical experimental conditions, for comparison.

2.4. Characterization

The sintered samples were ground and polished down to 1 μm using diamond pads of 220 grits and then polished by using 6 μm and 1 μm DP-suspension on polishing cloths. Fractured and thermally etched surfaces were gold coated and observed in an scanning electron microscopy (SEM, Hitachi S3200 N). To reveal the grain boundaries for the grain size estimation using the SEM, the pre-polished samples were thermally etched for 15 min at 1400 °C under argon (Ar) atmosphere in a tube furnace. For interface observations, sintered nanocomposites were break into fine powders then were studied using a transmission electron microscopy, (TEM, JEM2100, operated at 200 kV). Samples for TEM observations were prepared by using the chemical etching method as described in our previous work.[12]

2.5. Mechanical property evaluation

The Archimedes method was used to measure the densities of the samples (using distilled water), and the relative densities were calculated by dividing the apparent density by the theoretical density. In this study, 3.97 g/cm^3, 1.85 g/cm^3 and 2.21 g/cm^3 were used as the theoretical densities for Al_2O_3, CNTs and GNPs, respectively.[12] Vickers hardness testing was performed using a 5 kg force load for 15 s, and an average of five indents (equally spaced) was recorded for each sample. The flexural strength (σ_f) was measured by using the three-point bending technique, and the size of specimens was 21 (length) × 2 (breadth) × 2.5 mm (height). The bending span and the loading speed for the flexural strength testing were 16 mm and 0.5 mm/min, respectively. At least 4 bars were tested for each sample. The fracture toughness (K_{IC}) was evaluated using the single edge notched beam (SENB) method. 4 notched specimens with identical dimensions of 22 (length) × 2.6 ± 0.20 (breadth) × 2.4 ± 0.15 mm (height) were prepared using a diamond blade for each test, and the ratio of the notch depth to the specimen height (a/W) was maintained to ≈0.45–0.55 for all samples. Three-point bending tests were carried out using a loading speed of 0.01 mm/min and a span size of 16.5 mm.

3. Results

To assess the dispersion of GNTs in the Al_2O_3 nanopowder, TEM analyses were carried out prior to sintering. It is shown in Fig. 1 that the GNPs are stacks of 8–12 layers of graphene sheets with average thickness of 6–8 nm, and the Al_2O_3 nanoparticles are less than 20 nm. The GNPs and CNTs are both well-dispersed with the Al_2O_3 nanoparticles. This examination confirmed the success of our powder preparation processes adopted on this work. It is obvious that the water-based mixing strategy is an

Table 1
Theoretical and relative densities of the composites and their sintering conditions.

Sample	Matrix	GNP (wt%)	CNT (wt%)	Sintering Schedule	Relative density
$S_{0–0}$	Al_2O_3	0	0	1650 °C/40 MP/1 h/AR	98%
$S_{0–0.5}$	Al_2O_3	0	0.5	1650 °C/40 MP/1 h/AR	99.2%
$S_{0.5–0.5}$	Al_2O_3	0.5	0.5	1650 °C/40 MP/1 h/AR	99.3%
$S_{0.5–1}$	Al_2O_3	0.5	1	1650 °C/40 MP/1 h/AR	99.9%
$S_{1–1}$	Al_2O_3	1	1	1650 °C/40 MP/1 h/AR	99%
$S_{0.5–2}$	Al_2O_3	0.5	2	1650 °C/40 MP/1 h/AR	99%
$S_{0–2}$	Al_2O_3	0	2	1650 °C/40 MP/1 h/AR	97.5%
$S_{2–0.5}$	Al_2O_3	2	0.5	1650 °C/40 MP/1 h/AR	98%

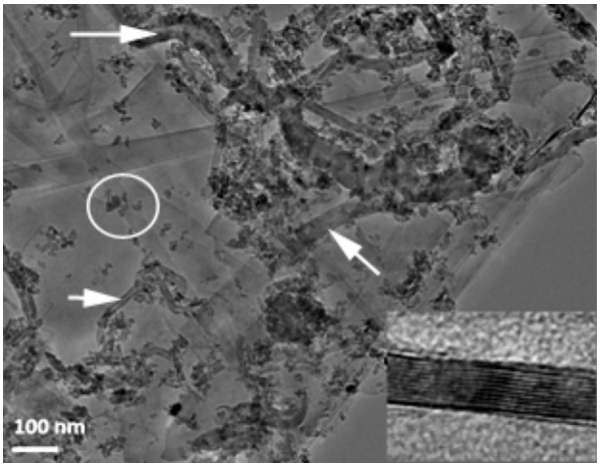

Fig. 1. TEM image of GNT and Al_2O_3 nanopowders showing dispersed CNTs (white arrows) and Al_2O_3 nanoparticles (white circle) on the GNP layers. High resolution TEM image of GNP (inset) showing stacks of 12 GNP layers.

environmentally friendly process and will not cause damage to the GNTs morphologies and structures during processing.

At various GNP/CNT ratios sintered under the same conditions, the densities of the resulting composites are presented in Table 1. At low GNT contents, the relative densities are very high, >99% .

In Fig. 2, the XRD data show the typical peaks of α-Al_2O_3 in all nanocomposites, without any detectable carbide phases, indicating no significant reactions between GNTs and Al_2O_3 during the sintering. At increased GNP/CNT ratios, a new peak is observed at 26.3° which corresponds to the crystalline graphite. The composite with 2 wt% GNP ($S_{2–0.5}$) revealed the clear graphitic peak at 26.3°; whilst almost no graphitic peaks for the composite containing 2 wt% CNT ($S_{0–2}$). The platelet structure of the GNPs makes the (0 0 2) planes dominant and easily detectable by XRD, compared with those containing the same amounts of CNTs.

Fig. 3 shows the SEM images of the fractured surfaces of monolithic Al_2O_3 and Al_2O_3-GNT nanocomposites. The fracture mode changed from inter-granular in the monolithic Al_2O_3 to blurry and glaze-like trans-granular mode in the composites. Meanwhile, the dispersion of GNTs within the fractured areas appears to be good (Fig. 3c). The laminate microstructures in Al_2O_3-GNT, shown in Fig. 3d, are thought to be related to the effect of GNTs in the grain refinment, which is also reported by Inam et al.[31] These laminated materials composed of layers with differently sized grains that were co-sintered together, which

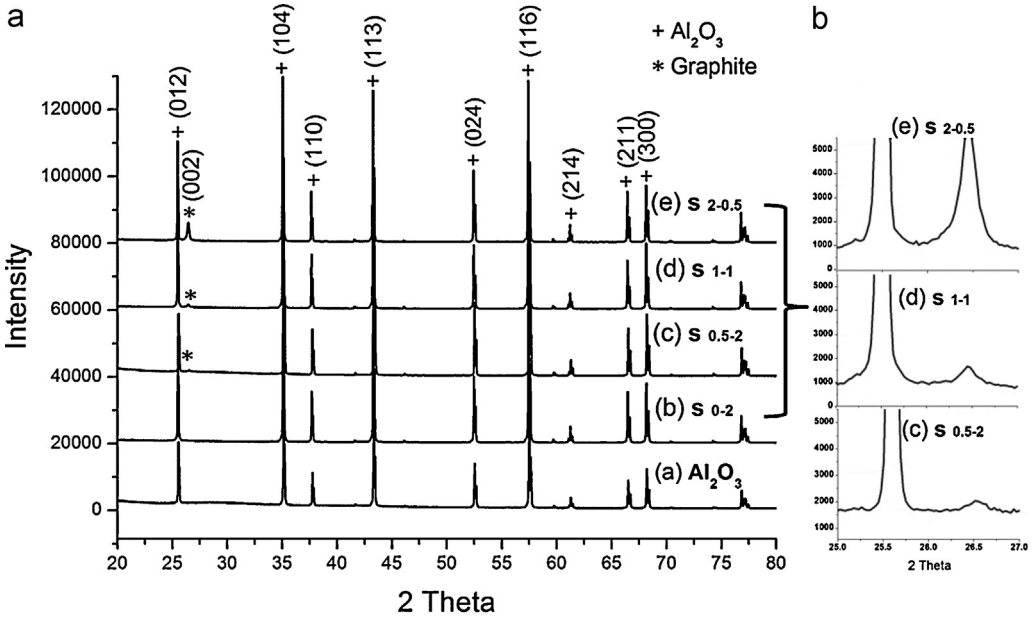

Fig. 2. XRD patterns of the monolithic Al_2O_3 and Al_2O_3-GNT nanocomposites with different GNP/CNT contents (a), and the zoomed sections of samples $S_{0.5–2}$, $S_{1–1}$ and $S_{2–0.5}$ (b).

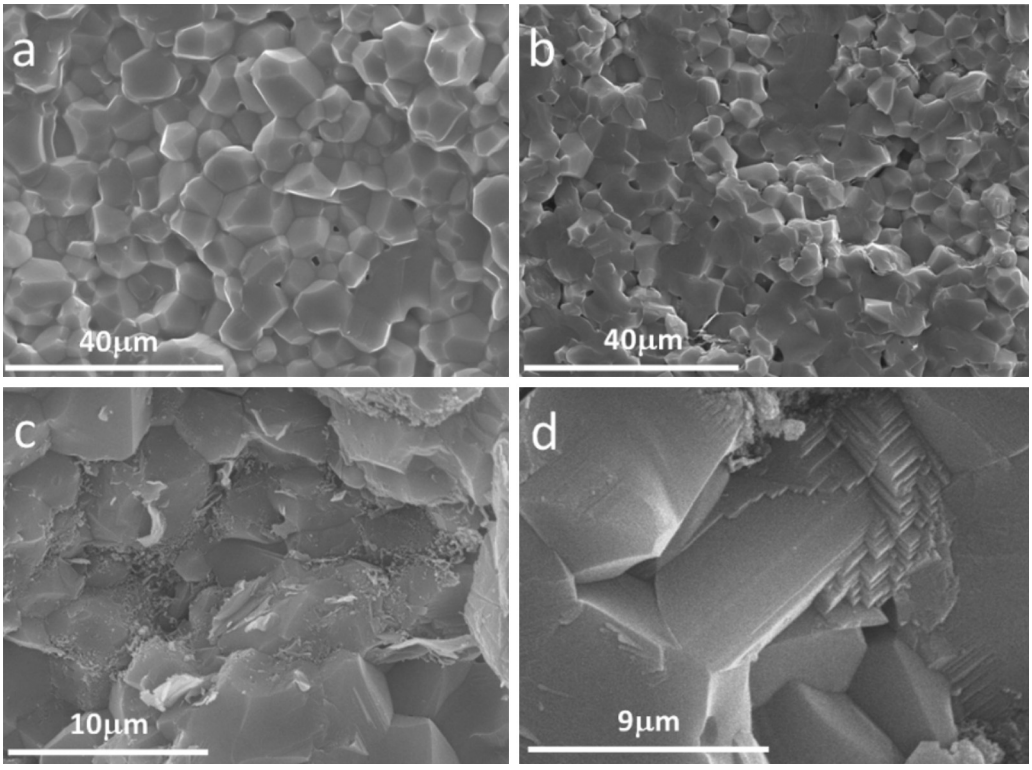

Fig. 3. SEM images of fractured surfaces: (a) monolithic Al_2O_3 exhibiting an inter-granular fracture mode, (b) $S_{0.5–1}$ showing a trans-granular fracture mode, (c) $S_{0.5–1}$ at higher magnification revealing the well-dispersed GNTs across the matrix, and (d) laminate structure in the Al_2O_3-GNT nanocomposites.

clearly illustrates the influence of GNTs on the microstructure. The structural features of the thermally etched surfaces of the monolithic Al_2O_3 and $S_{0.5–1}$ are shown in Fig. 4a and b, which reveals the grain refining effects of GNTs in the composites. The globular roughness in Fig. 4 is related to minute impurities from residues in the tube furnace which reacted with the sample surface during thermal etching. They do not affect the grain size study in this case.

Fig. 5 displays the hardness values vs the GNT contents. Compared with the plain Al_2O_3, the nanocomposites exhibit a slight increase by 6% in hardness, reached the highest value at low GNT content in specimen $S_{0.5–1}$. From $S_{0.5–1}$ to $S_{0.5–2}$ which contains 1 wt% more CNTs, the hardness sharply decreased by a 28%, and further reduction occurred with increased amounts of GNP of more than 0.5 wt%.

In order to find out the exact influence of GNPs and CNTs to the hardness, we redrew the hardness results in Fig. 6. By comparing Fig. 6a and b, it is shown that samples containing a fixed 2 wt% GNPs exhibited lower values at all CNT contents than those containing a fixed 2 wt% CNTs. Therefore, the increase of GNPs seems to have a stronger negative effect on the hardness than that of CNTs in the nanocomposites.

Fig. 7 shows that a 63% and a 12% increase in the fracture toughness and flexural strength have been achieved respectively in sample $S_{0.5–1}$, compared with the monolithic Al_2O_3, reaching 5.7 MPa $m^{1/2}$ and 424 MPa respectively. Fig. 7 also shows that at different GNP and CNT combinations, samples $S_{0.5–1}$, with the optimally combined additions of 0.5 wt% GNPs and 1 wt% CNTs, produced the highest fracture toughness and flexural strength. For samples $S_{0.5–1}$ to $S_{1–1}$, only a 0.5 wt% increase

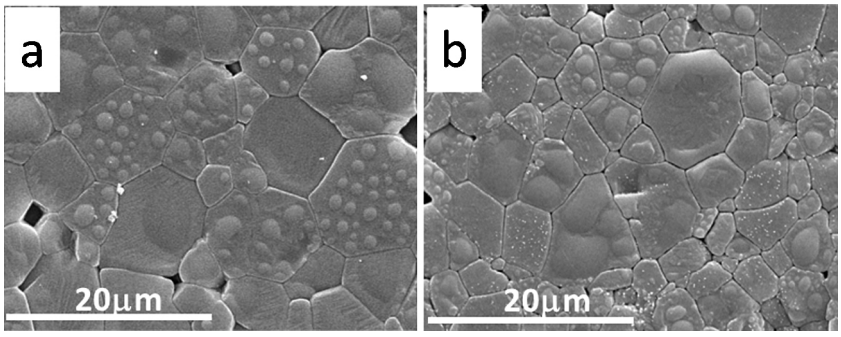

Fig. 4. SEM image of the thermally etched fractural surface of: (a) Al_2O_3, and (b) $S_{0.5–1}$.

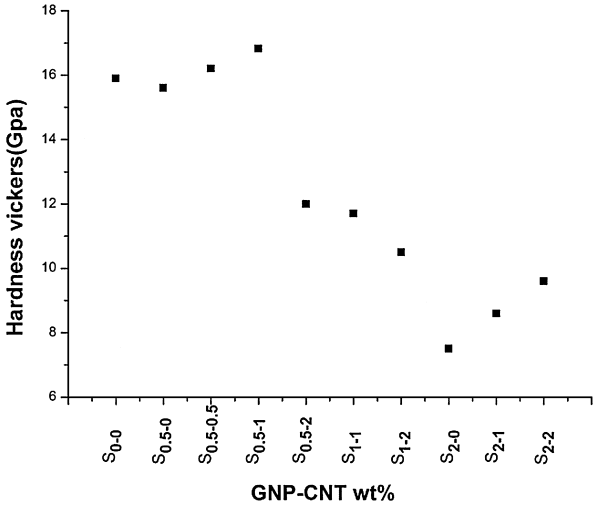

Fig. 5. Vickers hardness values of Al_2O_3-GNT nanocomposites at different GNP-CNT ratios.

in the GNP contents, the fracture toughness and flexural strength decreased by 38% and 35% respectively, which are much larger than their respective reductions from $S_{0.5-1}$ to $S_{0.5-2}$. With 1 wt% increase in CNTs in samples $S_{0.5-2}$, only recorded a 26% and a 6% reduction in these properties. Thereby, similar to the influence on the hardness, the GNPs seem to have much complicated effects than the CNTs in the fracture toughness and flexural strength of nanocomposites. This will be further discussed in Section 4.2.

4. Discussion

4.1. Structural features

The relative density in ceramic nanocomposites is an indirect indicator for assessing the dispersion of second phases in the matrix, as higher densities are indicative of better dispersion and normally resulting in better mechanical properties.[12,13] In Table 1, samples at specific GNP/CNT ratios exhibited relative densities of >99%. It seems that the dispersion of GNTs was quite successful, which are further supported by the SEM images (Fig. 3). The higher relative densities in composites than in the monnolithic Al_2O_3 in this work were also shown by other research.[11,32] It is possible that the inclusion of GNTs acted as a sintering agent due to their lubricating effect which might help better packing of the Al_2O_3 particles during the sintering process, thus resulting in the overall improved composite densities. Another possible reason for the higher density in the nanocomposites might be attributed to the 2D morphology of the GNPs in the matrix, as they have less an issue during the dispersion at low concentration compared with CNTs, thus may help to improve the final density. All the controlling factors in CNT's poor dispersion such as fibrous morphology, high aspect ratio, Van der Waals interaction and the presence of residue catalysts are not existed in the case of GNPs, therefore their dispersion process was easier than that of CNTs. However, with the addition of >0.5 wt% GNPs and >1 wt% CNTs, the densities of the composites started to decrease, in line with the associated difficulties in the GNT dispersion at higher contents.

In terms of the microtstructure, the GNT addition in the Al_2O_3 matrix refined the Al_2O_3 grains by forming laminated structures, as shown in Figs. 3b and 4 on the thermally etched surfaces. It is well-documented that the finer grains can lead to improved hardness and strenght of the composites, due to the grain boundary pining effect which impeded the dislocation movements.[33] However, grain refinment is obviously not the only effect observed in this context for the GNT addition in the nanocomposites. In Fig. 3a and b, the fracture morphology was found to change from inter-granular mode to trans-granular mode. This means that the GNT addition has also made the grain bounderies stronger, which would lead to other toughening mechanisms for the improved properties, which will be discussed in Section 4.3.

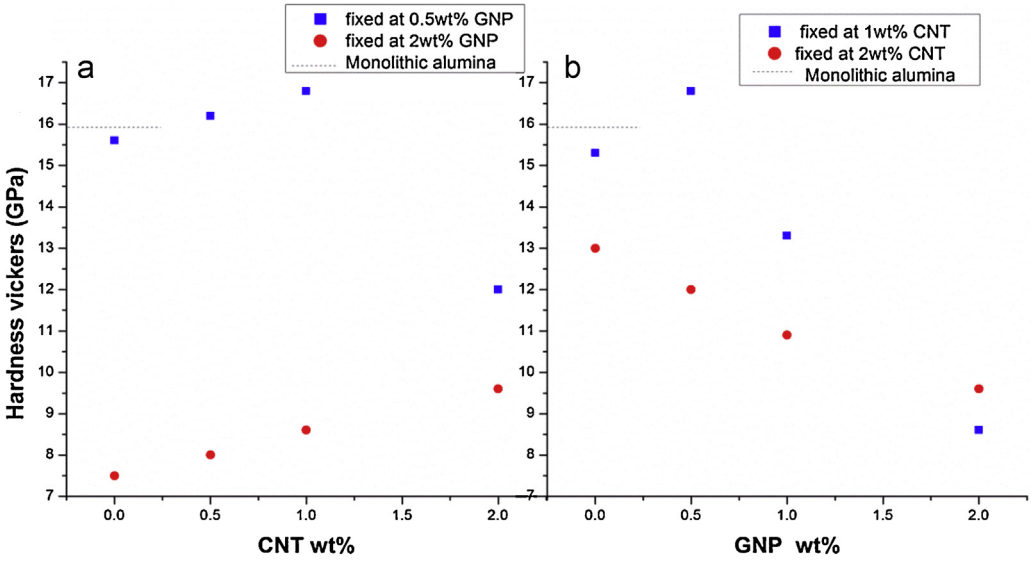

Fig. 6. Hardness values as a function of CNT wt% in the nanocomposites at different fixed GNP contents (a), and hardness values as a function of GNP wt% in the nanocomposites at different fixed CNT contents (b).

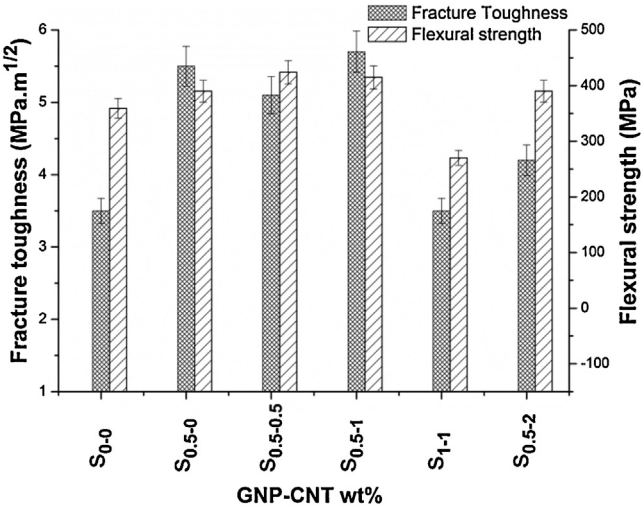

Fig. 7. Fracture toughness and flexural strength of the GNT-Al_2O_3 nanocomposites at different GNP/CNT ratios.

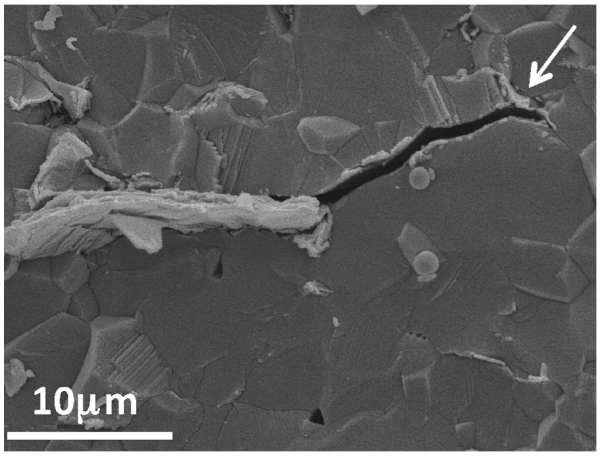

Fig. 8. SEM image of deboning of overlapped GNPs around the grain boundaries.

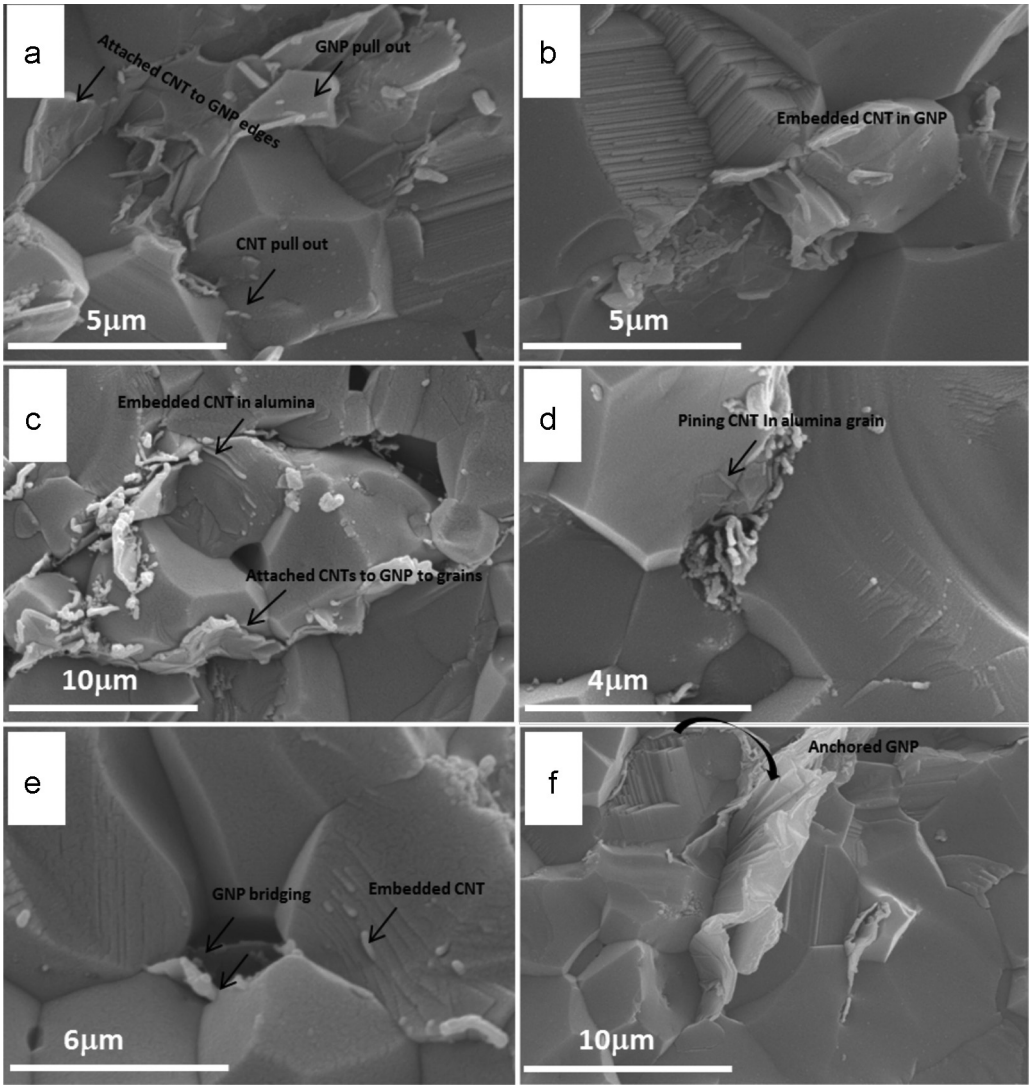

Fig. 9. SEM images of fractured surfaces of the GNT-Al_2O_3 nanocomposites for samples: (a and b) $S_{0.5–1}$, (c–e) $S_{0.5–0.5}$, and (f) $S_{0.5–0}$.

4.2. Fracture toughness and other mechanical properties

The fracture toughness was assessed by employing the SENB method which is considered as the most reliable technique for ceramic matrix composites. Sample $S_{0.5–1}$ revealed a 63% increase in the fracture toughness, as shown in Fig. 7. The previously reported Al_2O_3-CNT nanocomposites prepared by Ahmad et al.[12] have reached a 94% improvement in the fracture toughness over the monolithic Al_2O_3. The difference could be due to the different notch dimensions that were applied in samples for the SEND specimens, as small variations in notch dimension can lead to considerable changes in the fracture toughness.[34] However, in terms of flexural strengths, Fig. 7 also shows the relatively large improvement obtained here, a 15% improvement over monolithic Al_2O_3 in sample $S_{0.5–0.5}$, against a 6.4% improvement reported earlier in CNT-reinforced composites.[12]

Indeed, the higher fracture toughness values obtained in this study are believed to be due to the improved dispersion of GNTs with the matrix and increased contact areas between GNT and the Al_2O_3 matrix, which were achieved by adopting combined strategies during the mixing process. Firstly, allocating two weeks incubation time to CNT suspension allowed surfactant to be thoroughly adsorbed on the CNT surfaces, which led to a better dispersion in the Al_2O_3 matrix as described in our previous work.[12] Secondly, using both CNTs and GNPs as hybrid agents leads to better dispersion owing to their synergistic effect. Ultrasonic treatment during the mixing process was another factor to improve the GNT and Al_2O_3 nanoparticles dispersion during the mixing. This allows for more Al_2O_3 nanoparticles available to sandwiching with GNTs from the suspension, thereby more GNTs can be incorporated within the ceramic powder without re-agglomeration.

After examining different GNP-CNT combinations, we have also found out that the GNP contents exhibited a much severe influence than that of CNTs on the hardness, flexural strength and fracture toughness. This is possibly due to the agglomeration of GNPs in samples, rather than the GNP itself as a reinforcement, and demands further investigations in the future. Fig. 8 shows the fracture surface of a high GNP content sample, $S_{1–1}$. At >0.5 wt%, GNPs may be overlapped to form larger platelets of >200 nm thick, which could easily slide against each other and debound under stresses, as evident in Fig. 8. In contrast, CNTs are much smaller and have less contact areas with the grains, therefore exhibiting less sever effect. However, in Fig. 8, the crack ended up with smaller sheets of GNP (white arrow), opposite to GNP large flakes, which is an interesting feature observed for GNPs to prevent the crack propagation.

4.3. Reinforcement mechanisms

To investigate reasons behind the mechanical property improvements, further studies were carried out using SEM to investigate the microstructures of fractured surfaces. We also studied the CNT and GNP dispersion behaviour after sintering. Fig. 9 shows the SEM images of the freshly fractured surfaces of samples $S_{0.5–0}$, $S_{0.5–0.5}$ and $S_{0.5–1}$, respectively. It is found that conventional toughening mechanisms derived for fibre reinforced composites are also applicable to our Al_2O_3-GNT nanocomposites. CNTs and GNPs pull-out and bridging phenomena are visible in Fig. 9a and d, which are believed to have contributed to the effective improvement in the fracture toughness. In Fig. 9b, some CNTs are embedded on the GNP flake surfaces, which is another evidence for the strong synergetic effect between GNPs and CNTs. Fig. 9c also shows that the GNTs tend to accumulate around the grain boundaries. This might be the reason behind the grain refinement effect in the nanocomposites. As evidenced in Fig. 4, GNTs existing around the grain boundaries can effectively prevent the grain growth during sintering, and act as pining points to stop grain boundary movement during application. As shown in Fig. 9c and d, embedded CNTs around the grain boundaries, indeed pinned the Al_2O_3 grains together and strengthened the grain boundaries.

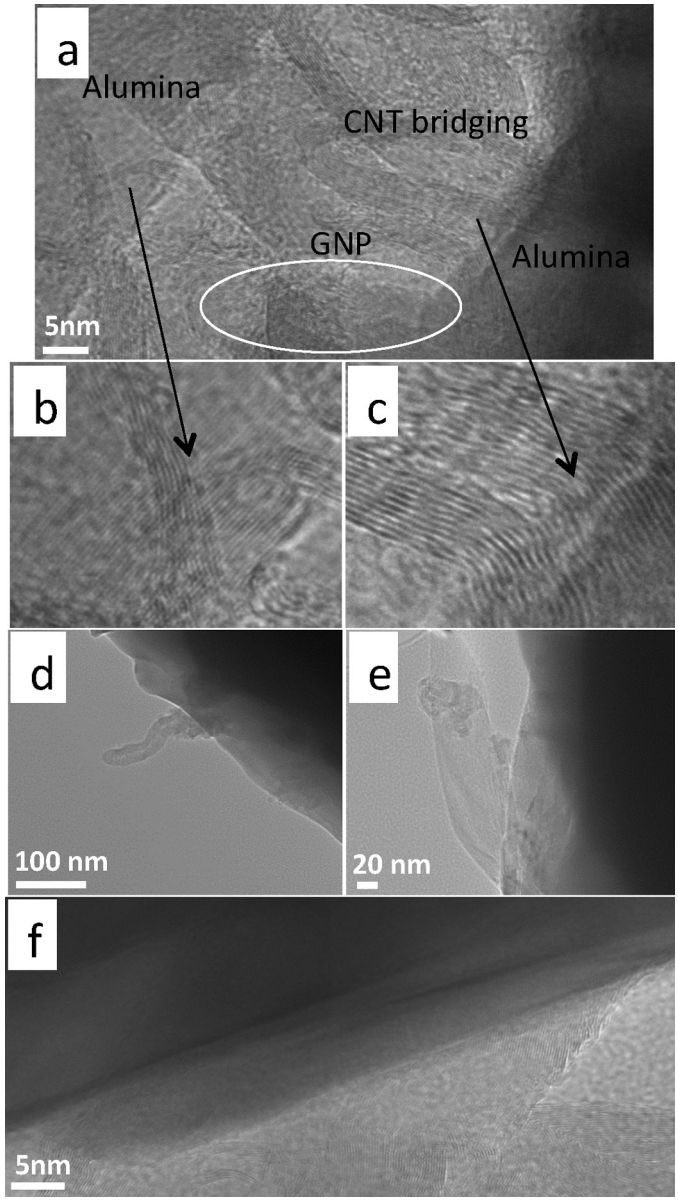

Fig. 10. TEM images of Al_2O_3-GNT nanocomposites showing the location of the CNPs and CNTs (a), enlarged images from selected areas of (a) (b and c), CNT and GNP pull out mechanism (d and e) and Al_2O_3-GNP interface (f).

As a result, these CNT strengthened grain-boundaries led to the changed fracture mode, from inter-granular to trans-granular in the nanocomposites, as shown in Fig. 3a and b. Primarily, the GNPs are more influencial to the former grain refinement, and the CNTs are more responsible for the interfacial strengthening. Fig. 9f shows a large GNP securely rolled along the Al_2O_3 grain, due to their flexibility, forming a large area of interface with matrix. Such anchoring mechanism can lead to increased interfacial frictions between the GNPs and the matrix, and the required energy to pull out such GNPs is expected to be higher than that for CNTs. Therefore, the fracture occurred through the Al_2O_3 grains rather than along the grain boundaries, as shown in Fig. 9f. These results mean that the CNTs and GNPs have played different roles in improving the fracture toughness, due to their different microstructures. GNPs increased the required pull out energy during fracture by anchoring around the Al_2O_3 grains and produced higher contact area with grains; whilst CNTs bridged the grains due to their higher aspect ratio. It is believed that CNTs can be stretched much longer than GNPs before collapsing during the crack propagation, thereby contributing more to the bridging effect. These roles are complementary with each other at appropriate concentrations, allowing for absorbing more energy during crack propagations.

Our TEM study (Fig. 10a–f) also confirmed the bridging and pull-out reinforcing mechanisms. Fig. 10a shows a CNT bridging across two Al_2O_3 grains, and Fig. 10d and e displays a CNT and a GNP being pulled out from the Al_2O_3 grains, respectively. High resolution images from the selected area in Fig. 10a exhibits the existence of embedded CNTs on the GNP surfaces, in consistence with the SEM results shown in Fig. 9b. In Fig. 10f, firmly attached CNTs and GNPs to the matrix are shown, indicating their strong interfacial connection with the matrix, thereby leading to increased toughness in the composites.

5. Conclusion

Al_2O_3 ceramics reinforced by hybrid GNT nanoreinforcements were prepared via a combination of wet dispersion and probe sonication technique. At low additions, high performance Al_2O_3 nanocomposites were obtained by hot-press, without any damage to the GNT reinforcements. The CNTs attached to the GNP surfaces and edges during the mixing process helped their deagglomeration and homogenous dispersion within the matrix. At higher additions where dispersion became a problem, GNPs exhibited much severer negative effect than the CNTs on the mechanical properties. The GNPs contributed more to the grain refinements and the CNTs contributed more to improve the interfacial strengths. Meanwhile, the GNPs were primarily increased the pull-out energy whilst CNTs were found to bridging the grains and pinning the grain boundary movement, thereby complementarily improved the toughness and fracture strength of the composites, reaching 5.7 MPa $m^{1/2}$ and 424 MPa respectively.

Acknowledgements

BY thanks the University of Exeter for scholarship support, and YZ thanks EPSRC for financial support.

References

1. Liu BQ, Huang CZ, Sun AL. *Adv Mater Res* 2012;**500**:634–9.
2. Mozalev A, Sakairi M, Takahashi H, Habazaki H, Hubálek J. *Thin Solid Films* 2014;**550**:486–94.
3. Martin CA, Lee GF, Fedderly JJ. US Patent 8, 387, 510 (2013).
4. Baron B, Kumar C, Le Gonidec G, Hampshire S. *J Eur Ceram Soc* 2002;**22**:1543–52.
5. Ipek M, Zeytin S, Bindal C. *J Alloys Compd* 2011;**509**:486–9.
6. Bartolomé JF, Pecharromán C, Moya JS, Martín A, Pastor JY, Llorca J. *J Eur Ceram Soc* 2006;**26**:2619–25.
7. Hansson T, Warren R, Wasen J. *J Am Ceram Soc* 1993;**76**:841–8.
8. Ostertag CP. *Mater Sci Eng A* 1999;**260**:124–31.
9. Yamamoto G, Omori M, Hashida T, Kimura H. *Nanotechnology* 2008;**19**:315708.
10. Wei T, Fan Z, Luo G, Wei F, Zhao D, Fan J. *Mater Res Bull* 2008;**43**:2806–9.
11. Inam F, Peijs T, Reece MJ. *J Eur Ceram Soc* 2011;**31**:2853–9.
12. Ahmad I, Cao H, Chen H, Zhao H, Kennedy A, Zhu YQ. *J Eur Ceram Soc* 2010;**30**:865–73.
13. Fan J, Zhao D, Wu M, Xu Z, Song J. *J Am Ceram Soc* 2006;**89**:750–3.
14. Estili M, Kawasaki A, Sakka Y. *Adv Mater* 2012;**24**:4322–6.
15. Fan J-P, Zhuang D-M, Zhao D-Q, Zhang G, Wu M-S, Wei F, et al. *Appl Phys Lett* 2006;**89**:121910–3.
16. Fan Y, Wang L, Li J, Sun S, Chen F, Chen L, et al. *Carbon* 2010;**48**:1743–9.
17. Wang K, Wang YF, Fan ZJ, Yan J, Wei T. *Mater Res Bull* 2011;**46**:315–8.
18. Kun P, Tapasztó O, Wéber F, Balázsi C. *Ceram Int* 2012;**38**:211–6.
19. Kvetkova L, Duszova A, Hvizdos P, Dusza J, Kun P, Balazsi C. *Scr Mater* 2012;**66**:793–6.
20. Liu J, Yan H, Reece MJ, Jiang K. *J Eur Ceram Soc* 2012;**32**:4185–93.
21. Dusza J, Morgiel J, Duszová A, Kvetková L, Nosko M, Kun P, et al. *J Eur Ceram Soc* 2012;**32**:3389–97.
22. Balazsi C. *J Korean Ceram Soc* 2012;**49**:352–62.
23. Ramirez C, Figueiredo FM, Miranzo P, Poza P, Osendi MI. *Carbon* 2012;**50**:3607–15.
24. Liu J, Yan H, Jiang K. *Ceram Int* 2013;**39**:6215–21.
25. Shin MK, Lee B, Kim SH, Lee JA, Spinks GM, Gambhir S, et al. *Nat Commun* 2012;**3**:650.
26. Stankovich S, Dikin DA, Dommett GH, Kohlhaas KM, Zimney EJ, Stach EA, et al. *Nature* 2006;**442**:282–6.
27. Kuilla T, Bhadra S, Yao D, Kim NH, Bose S, Lee JH. *Prog Polym Sci* 2010;**35**:1350–75.
28. Khan U, May P, O'Neill A, Coleman JN. *Carbon* 2010;**48**:4035–41.
29. Layek RK, Samanta S, Nandi AK. *Carbon* 2012;**50**:815–27.
30. Chen S, Yeoh W, Liu Q, Wang G. *Carbon* 2012;**50**:4557–65.
31. Inam F, Yan H, Peijs T, Reece MJ. *Compos Sci Technol* 2010;**70**:947–52.
32. Milsom B, Viola G, Gao Z, Inam F, Peijs T, Reece MJ. *J Eur Ceram Soc* 2012;**32**:4149–56.
33. Rice RW. *Mechanical properties of ceramics and composites: grain and particle effects*. United States: Taylor Francis Inc; 2000.
34. Nishida T, Hanaki Y, Pezzotti G. *J Am Ceram Soc* 1994;**77**:606–8.